1999

Flow convergence and stability at a tidal estuarine front: Acoustic Doppler current observations

John M. Brubaker
Virginia Institute of Marine Science, brubaker@vims.edu

John H. Simpson
University of Wales

JOURNAL OF GEOPHYSICAL RESEARCH, VOL. 104, NO. C8, PAGES 18,257–18,268, AUGUST 15, 1999

Flow convergence and stability at a tidal estuarine front: Acoustic Doppler current observations

John M. Brubaker

School of Marine Science, Virginia Institute of Marine Science, College of William and Mary, Gloucester Point

John H. Simpson

Marine Science Laboratories, School of Ocean Sciences, Menai Bridge, University of Wales, Anglesey

Abstract. Characteristics of the flow field in an estuarine frontal zone have been investigated in a field study in the lower James River estuary. Underway sampling with an acoustic Doppler current profiler (ADCP) on repeated transects across the front provided information on the structure of the flow field near the front and its evolution in time. As this tidal intrusion front advanced up the estuary during the flooding tide, prominent and consistent features in the velocity field included a localized zone of convergent flow beneath the visible surface line and a stratified shear layer just upriver of the front. Within the shear layer between the buoyant surface water and the faster, higher-salinity undercurrent, gradient Richardson number estimates suggest that the flow was at or near the threshold for shear instability. Another shear-type gradient in the flow field, the across-front variation of the along-front velocity component, strengthened over a sequence of transects, with intensity increasing toward the surface. Tracking of the front was then interrupted when the identifying line of foam and accumulated material on the surface, previously sharp and well defined, broke up and dispersed to such an extent that the visible signature of the front was lost temporarily. A visible frontal expression later reappeared, and propagation upriver continued. Lower bound estimates of downwelling flow in the frontal zone were determined by continuity considerations.

1. Introduction

Fronts, zones of locally intensified horizontal gradients in water properties, are frequently observed in open ocean, coastal, and inland waters, spanning a broad range of space scales and timescales. Although the history of concerted research effort on fronts is comparatively brief, the potential physical and ecological significance of fronts is now widely appreciated. *Mann and Lazier* [1996], for example, discuss physical and biological processes associated with several classes of front. In this paper, we present results from an observational investigation of the velocity field at a moving tidal front in a partially mixed estuary.

Typical characteristics of fronts observed within and near estuaries include relatively small spatial scales, evolution over tidal timescales, and buoyancy effects controlled by salinity variations. Coriolis effects on the dynamics of such small-scale fronts may be expected to be negligible [*Garvine*, 1979]. *Largier* [1993] provides an overview of the role of estuarine fronts, while reviews by *O'Donnell* [1993], *Bowman* [1988], and *Simpson and James* [1986] highlight the considerable progress that has been made in identifying various mechanisms controlling the formation and maintenance of these fronts. Currently, however, our understanding of frontal-scale structure and dynamics is relatively primitive, and progress is limited by the lack of direct observations of the velocity field.

For estuarine fronts the velocity structure at vertical scales of order 1–10 m and horizontal scales of order 10 to 100 m is of particular interest, lying between regimes controlled at larger scales by basin dimensions and at smaller scales by viscous, dissipative processes. At the intermediate scales, buoyancy and inertial forces are dominant, and these are central to frontal dynamics [*McClimans*, 1988]. Typically, fronts in estuaries are ephemeral, and often the frontal structure undergoes translation and/or deformation, presenting significant obstacles to observational programs. The problems are exacerbated if, as in some environments, the occurrence of fronts is erratic and in unpredictable locations. *Simpson and James* [1986] outline some of the difficulties in obtaining near-synoptic maps of scalar properties in frontal systems; velocity observations are potentially even more difficult and correspondingly rare [*O'Donnell*, 1993]. Instrumentation arrays deployed in innovative configurations by *Marmorino and Trump* [1996] and *O'Donnell* [1997] have provided critical velocity information in moving frontal zones, and a characterization of the complex multidimensional, multiple-scale variability in velocity fields associated with various kinds of estuarine fronts appears to be in an early but promising stage of development.

Recent observations in the partially mixed James River estuary, a tributary to the Chesapeake Bay, have documented the existence of an estuarine front in the vicinity of Newport

Paper number 1999JC900117.
0148-0227/99/1999JC900117$09.00

News Point (Figure 1), which has proved to be a persistent and, to some extent, predictable feature of the region. Although its structure and motion are variable and complex, the front forms consistently just off Newport News Point when the tidal current over Hampton Flats in early flood converges with the flow in the deeper channel southwest of the point, which is lower in salinity and still in late ebb. The role of river geometry and tidal phasing in the origin of the front is discussed by *Kuo et al.* [1990a]. Dye studies in the James reported by *Kuo et al.* [1988] have established that surface water of the incoming flood current plunges at the front, proceeding upriver beneath a buoyant layer of lower salinity. This flow structure, salient features of which are indicated schematically in Figure 2, is characteristic of tidal intrusion fronts, a class of estuarine front which has been reviewed by *Largier* [1992] and described by *Simpson and Nunes* [1981] in the context of a much more highly stratified estuary. Similar fronts have also been observed in bar-built estuaries [*Largier and Taljaard*, 1991]. The James River front has been observed to evolve through several stages as it moves upriver during the first half of the flood phase, with the leading edge frequently exhibiting the characteristic "V" shape reported by Simpson and Nunes. *Marmorino and Trump* [1996] have towed an acoustic Doppler current profiler (ADCP) along one side of this front with two beams in a horizontal plane, profiling across the front. With this approach, information on the three-dimensional structure of the front was derived, and high resolution of across-front gradients in the very near field of the front was achieved. Further description of the frontal system and the regional hydrography has been reported by *Ruzecki and Hargis* [1989], *Byrne et al.* [1987], *Kuo et al.* [1988, 1990a, b], and *Mann* [1988].

In the study reported here we have investigated the evolving, intermediate-scale velocity structure in this estuarine frontal zone as it advanced upriver over variable bottom topography with the tidal flood current. Following a description of the observational setting and data in section 2, results presented in section 3 characterize the general patterns observed in the velocity field and the salinity-controlled stratification in the vicinity of the front. High-gradient regions of the velocity field are examined in section 4, including vertical shear upriver of the front and horizontal convergence and horizontal shear across the front. Stability considerations and downwelling at the front are discussed in section 5.

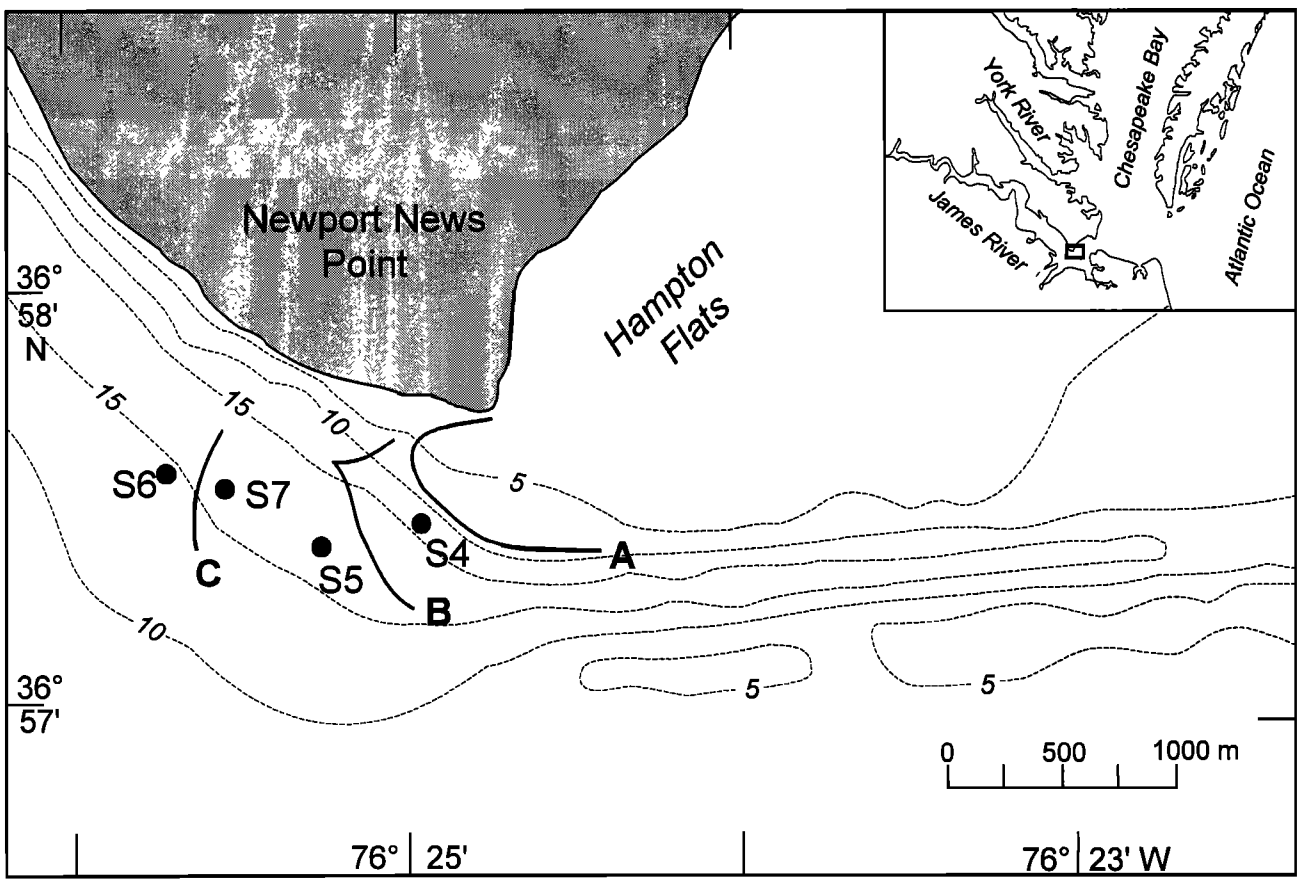

Figure 1. The study site in the James River estuary, part of the lower Chesapeake Bay area (inset), near Newport News Point. Curves A-C indicate the approximate position of the visible frontal boundary at 1515, 1536, and 1637 LT, based on observations relative to buoys and onshore landmarks. Between 1519 and 1600, acoustic Doppler current profiler (ADCP) transects X5–X9 crossed the front at locations between stations S4 and S5, and conductivity-temperature-depth (CTD) profiles were acquired at the beginning (S4) and at the end (S5) of X7. CTD profiles at S6 and S7 were sampled at the beginning and end of transect X10, which crossed the front when it was at curve C. Dashed contours indicate depth (meters).

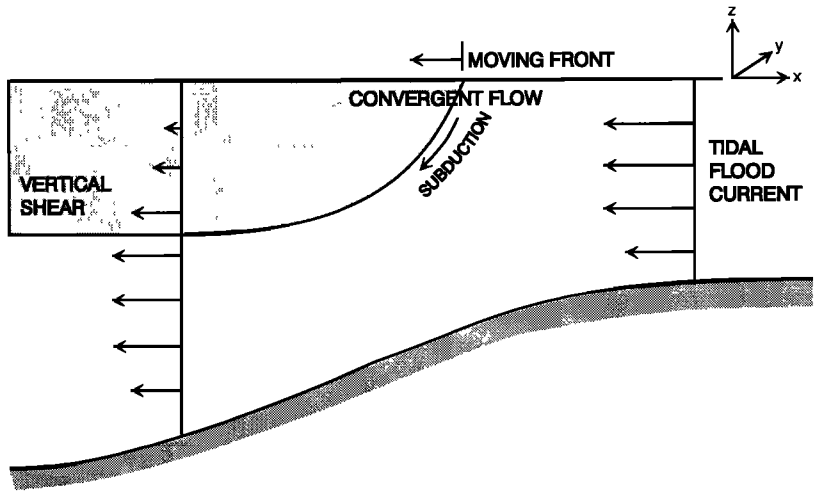

Figure 2. Schematic representation of a tidal intrusion front indicating velocity profiles on either side of the front. In the present study, characteristics of near-surface convergence, vertical shear between the buoyant layer (shaded) and the intruding undercurrent, and horizontal shear of along-front flow at the front have been investigated through ADCP observations.

2. Field Experiment

This study is based on shipboard observations, acquired near a moving frontal system in the vicinity of Newport News Point in the James River (Figure 1), exploiting the underway sampling capability of a bottom-tracking ADCP. During this particular study, the identifying visible manifestation of the front was primarily a thin line of foam and accumulated grass and debris; on other occasions the front has also been marked by a color change and/or surface roughness transition. Measurements were made from the 14-m R/V *Langley* in two sampling modes: on transects crossing the front orthogonal to its surface expression and at pairs of stations bracketing the front. At the stations, vertical profiles of temperature and salinity were sampled using a hand-lowered conductivity-temperature-depth (CTD) instrument (Applied Microsystems STD-12), and ADCP data were recorded during the CTD casts.

Along the transects, several hundred meters in length, vertical profiles of velocity were acquired underway with a 1.2-MHz narrowband ADCP (model DR, RD Instruments). The transducers were 1.7 m below the water surface, the beam angle was 30° off vertical, and the vertical bin length and pulse length were both 1 m. Groups of five pings, at a ping rate of 5 Hz, were averaged in the ADCP and sent to the data acquisition computer where, within an overall sampling cycle of 20 s, an ensemble representing 35–40 individual pings was accumulated, processed, and recorded. For each ensemble, bottom-track velocities were subtracted from directly measured horizontal components to obtain water flow velocities. Trade-offs between spatial resolution and velocity uncertainty for underway ADCP sampling are discussed in the appendix.

Position data were provided at 2-s intervals by a Del Norte Microwave Trisponder system with a specified range uncertainty of ±1 m and a fix uncertainty of ±1 to ±4 m, dependent upon the geometrical arrangement of shore-based remote stations relative to the vessel position. As a check on ADCP bottom tracking, independent estimates of boat velocity were computed from microwave position data. In comparing the velocities, several considerations arise: (1) Across the 20-s time interval of individual ADCP ensembles, position fix uncertainty was a significant fraction of the distance traveled, introducing considerable noise in the microwave-based velocity estimates at that timescale. (2) The transects of this study were characterized by significant and systematic variations in boat velocity, presumably reflecting the influence of surface circulation associated with the front (as discussed in section 4.2 and shown in Figure 7). (3) During these variations even small errors in time synchronization between the two systems would lead to serious discrepancies in velocity estimates. Thus for the primary calibration check of bottom tracking only multi-ensemble segments with relatively steady velocity were considered, in particular, the segments of transects 6 and 7 prior to encountering the front. Following *Joyce* [1989], a misalignment angle α and scaling factor $(1+\beta)$ were determined, with the following results: $\alpha = 0.14°$ and $\beta = -0.0022$ heading downriver on transect 6, and $\alpha = 2.55°$ and $\beta = 0.0093$ heading upriver on transect 7. As a secondary comparison, because the steps in boat velocity shown in Figure 7 were of interest in this study, corresponding microwave-based records of the across-front velocity component were formed and subtracted from the bottom-track records. For each transect the series of velocity differences had a mean value of 1.5 cm s^{-1} or less and a standard deviation of typically 3 cm s^{-1}. In view of the noise noted above for fix-based velocities at this 20-s timescale, this agreement appeared to be reasonable. Overall, in consideration of the above results for bottom tracking over segments of steady and unsteady boat velocity and the estimated statistical uncertainty of 2.2 cm s^{-1} in the ADCP data (see the appendix), the ADCP velocities were regarded as acceptable without postcruise correction.

Observations reported here began in the early afternoon of November 2, 1987, under clear skies and in a gentle breeze (less than 10 knots), good conditions for front visibility. By 1515 LT, a sharply defined front was positioned on the shallow side of a relatively steep bottom slope, as indicated

by curve A in Figure 1. As the front moved upriver into deeper water (to the left in Figure 1), cross-front transects X5–X7 were executed (travel was upriver on all odd-numbered transects and downriver on even ones), and CTD profiles were sampled at station S4 before transect X7 and at station S5 after transect X7, so that S4 was on the seaward side and S5 was on the upriver side of the front. At the end of this sampling, 1536 LT, the location and shape of the front as delineated by the visible line at the surface were approximately as indicated by curve B in Figure 1. Shortly thereafter, the visual definition of the front deteriorated significantly and abruptly. Transects X8 and X9 were sampled between 1545 and 1600 LT across the indistinct and dispersed remains of the previously well-defined surface boundary line.

By approximately 1620 LT, 0.5 km upriver from the breakup of the surface features, an extended, coherent frontal boundary was again observed. When it had advanced to the location indicated by curve C in Figure 1, bracketing CTD casts were taken at stations S6 and S7, at the beginning and end of transect X10.

The orientation of the front changed gradually as it progressed up the estuary, and velocity components (u, v, w) are specified herein with respect to a local coordinate system (x, y, z) aligned with across-front (x) and along-front (y) directions, as indicated in Figure 2. ADCP compass data along transects were in good agreement with course determinations based on position fixes from the Del Norte system.

3. Velocity Field and Stratification

As noted in section 1, the earliest signs of this frontal system usually appear when the flow in the main channel south of Newport News Point is near the end of the ebb phase. On the day of this study, the predicted time of slack before flood at this location was 1447 LT. Observational results summarized here were acquired within the first half of the tidal flood current, during which time there were two separate intervals when a sharply delineated frontal line on the surface was followed upriver. During a transition phase between these two intervals, tracking of the front was interrupted when its identifying visual surface expression broke up, spread, and temporarily disappeared.

3.1. Phase 1: Early Flood Current Over Downslope

Differences in the vertical structure of the water column on opposite sides of the front during the first phase are illustrated by profiles of temperature, salinity, density, and velocity shown in Figure 3. When the front lay along curve B in Figure 1, conditions on the seaward side, at station S4, were relatively uniform in the vertical, as shown in Figure 3b. Density, represented by σ_t, varied less than 0.2 kg m^{-3} over the water column, and the 60-s average velocity profile, acquired during the CTD cast, shows that the flood current flowing westward toward the front exhibited little variability about an underlying, characteristic tidal flow profile. Maximum speeds were approximately 50 cm s^{-1}.

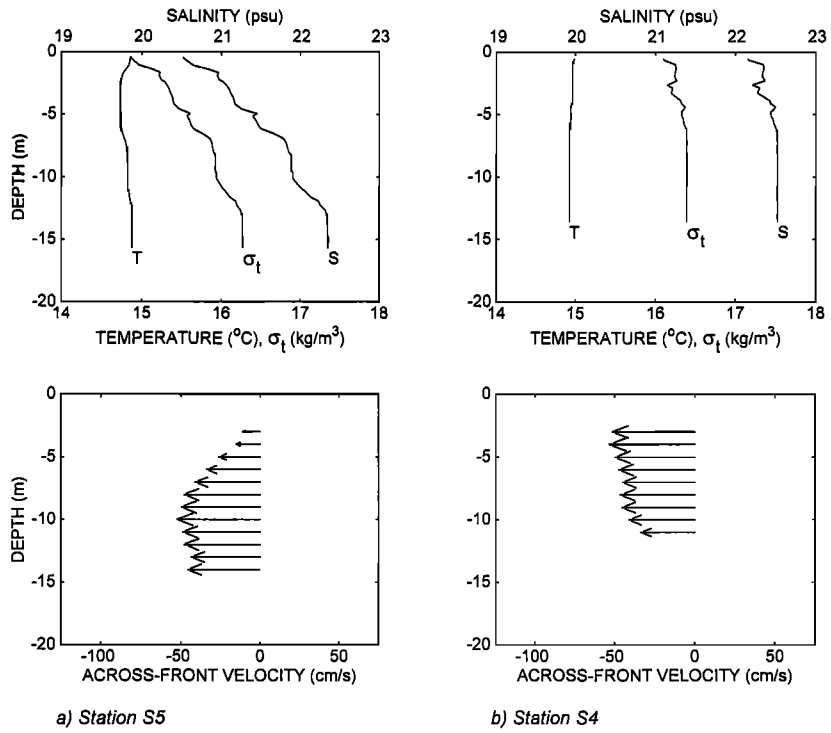

Figure 3. Observed vertical structure on opposite sides of the front at (a) station S5 and (b) station S4 when the front was located near curve B in Figure 1. Vector plots represent 60-s average ADCP velocity data acquired during the corresponding CTD cast, and orientation of the vectors corresponds to the representation in Figure 2. Statistical uncertainty of the velocity data is 1.2 cm s^{-1}. psu, practical salinity unit.

In contrast, at station S5 (Figure 3a) on the other side of the front the water column was substantially more stratified, with a top-to-bottom density difference, controlled by the salinity distribution, of 1.4 kg m^{-3}. The gross structure consisted of two distinct, nearly homogeneous layers beneath a continuously stratified surface layer in the upper 6 m. The deep layer density was approximately the same as the near-surface density of the approach flow at station S4. The velocity profile was fundamentally different from that at S4, with strong shear of the opposite sense in the upper stratified layer where density and velocity both varied linearly with depth.

A more complete view of the velocity field in a vertical plane intersecting the front is provided by sets of sequential ADCP ensembles sampled underway during cross-front transects, shown in Figure 4. In each transect the most seaward profile is on the right; transects with negative ensemble numbers began on the seaward side of the front. This direct vector representation of the data exposes limitations of the horizontal resolution of the 20-s ensembles, relative to the sharpness of the front; implications will be noted in section 5.3. (An alternative view of the across-front flow field, along with velocity gradient fields, is presented in section 4.) When the front was located near the 10-m isobath upriver of curve A in Figure 1, transect X5 crossed it at a vessel speed of approximately 2 m s^{-1}. Each individual 20-s ensemble for this transect thus represents an average over a horizontal interval of about 40 m. Along this transect, as shown in Figure 4, the flood current approaching the front remained fairly uniform as it flowed into increasing water depth (ensembles 98–100), meeting the front on the slope. The transition between ensembles 100 and 101 coincided with the visible frontal boundary (as indicated by the symbol "F" in the vector plot), and once the front was crossed, little further change was observed over the next 200 m spanned by ensembles 101–105. On the upriver side of the front the near-surface current was only weakly flooding.

The structure of the across-front velocity field was substantially the same in subsequent transects X6 (not shown) and X7, when the front was over deeper, flatter bottom. Again, the abrupt change in velocity structure (between ensembles 33 and 34 in transect X7) corresponded to crossing the conspicuous surface delineation of the front. In the 14 min between the X5 and X7 crossings, the front had moved upriver approximately 250 m, providing an estimate of 30 cm s^{-1} for the average frontal propagation speed during this phase. Thus the front and the water on both sides of the front were all moving upriver in approximately the same direction, the water on the seaward side near the top of the ADCP profile at speeds of 40–50 cm s^{-1} and the water on the opposite side at 0–10 cm s^{-1}. Relative to the moving front, the water on the seaward side was approaching the front at 10–20 cm s^{-1}, and the water on the opposite side was approaching the front at 20–30 cm s^{-1}, indicating two-sided convergence in the frontal zone.

3.2. Phase 2: Transition

Ten minutes after the X7 crossing, we prepared to execute transect X8 and noted that significant disintegration of the foam line had occurred, although a broad swath of scattered remnants could be discerned. In contrast to the apparent

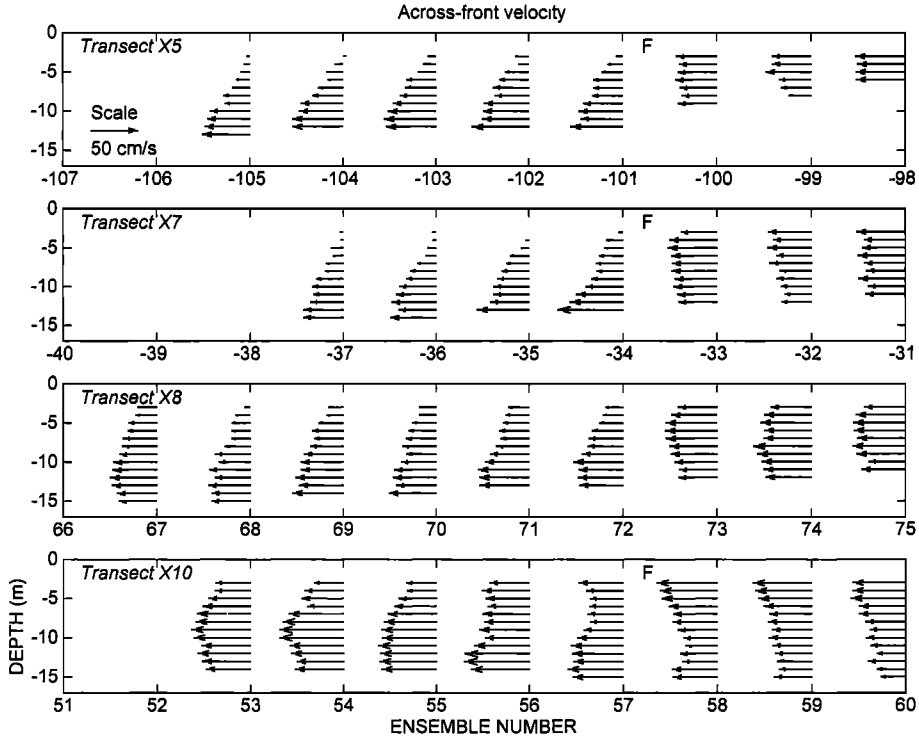

Figure 4. ADCP velocity profiles acquired underway during transects across the frontal zone, presented as sets of consecutive 20-s ensembles. Transect X5 crossed the front at 1519 LT, X7 crossed at 1533 LT, X8 crossed at 1547 LT, and X10 crossed at 1637 LT. In transects where a sharp visible frontal boundary at the surface was observed, its correspondence with ADCP ensembles is indicated by the symbol "F" in the plots. During transects X8 (and X9, not shown) a distinct front line was not observed. Statistical uncertainty of the velocity data for each ensemble is 2.2 cm s^{-1}.

changes at the surface, however, the frontal structure in the velocity field measured below the surface during X8 is shown in Figure 4 to have remained relatively sharp (with respect to the horizontal resolution of the ADCP data) and bracketed by ensembles 72 and 73. During transect X9 (not shown), in which the front was crossed 6 min after X8 and in the opposite direction, conditions were qualitatively similar to those observed during X8 with respect to both the continued frontal character of the subsurface velocity field and the lack of visual definition of the front at the surface.

Note that by the time of transect X8 the flood current in the near-surface water on the fresher side of the front had begun to strengthen (compare ensembles 34–37 of X7 with ensembles 72–69 of X8). Just seaward of the front, the vertical structure of the flow changed slightly from transect X5 (ensemble 100) to X7 (ensemble 33) to X8 (ensemble 73), suggesting a downward migration of the level of maximum across-front flow approaching the front. Associated cross-front convergence and other features of the evolving flow structure can be seen more clearly and quantitatively in terms of computed velocity gradient fields, which are presented in section 4. In section 4 we also consider the lateral (across front) shear of the along-front velocity ($\partial v/\partial x$), which had increased significantly across the front at the time of transect X7, just before the observed breakup of the foam line.

3.3. Phase 3: Stronger Flood Current and Reestablished Surface Signature

Approximately 30 min after X9 and several hundred meters up the river, a sharp and coherent frontal line of foam and accumulating debris could once again be clearly seen. When it had advanced to the approximate location indicated by curve C in Figure 1, station S6, transect X10, and station S7 were sampled. As before, the vertical structure on the seaward side (station S7, Figure 5b) was quite uniform in scalar properties, and velocity decreased moderately with depth. On the opposite side at station S6 (Figure 5a), density and velocity increased linearly with depth through the upper layer, and velocity decreased with depth in the homogeneous lower layer.

As in phase 1, the front was easily tracked by its surface signature propagating up-estuary but now over relatively flat bottom. The subsurface velocity field for transect X10 is shown in Figure 4, indicating that by this time the overall flow had increased considerably, although the difference in velocity magnitude across the front was approximately as in phase 1. Consistent with the renewed character of the front, in X10 the maximum velocity approaching the front on the seaward side (ensemble 58) was at the top of the ADCP profile, reversing the downward migration noted in section 3.2.

4. Velocity Gradient Fields

The across-front velocity field $u(x,z)$ measured during transects X5, X7, and X8 (when the front was moving between curves A and B in Figure 1) is shown in Figure 6a. This representation illustrates the gross frontal-zone structure of the flow field and indicates qualitatively the patterns of shear and convergence in this velocity component. Now we consider quantitative estimates of gradients in the velocity field near the front, specifically the vertical shear and across-front convergence of the across-front velocity, $\partial u/\partial z$ and $-\partial u/\partial x$, respectively, and the across-front shear of the along-front velocity, $\partial v/\partial x$.

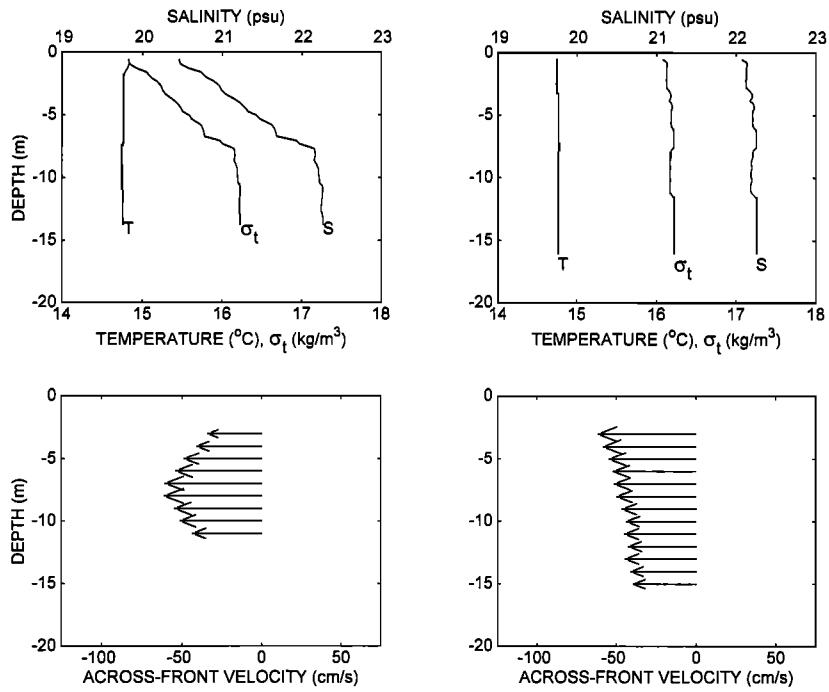

Figure 5. Observed vertical structure on opposite sides of the front at (a) station S6 and (b) station S7 when the front was located near curve C in Figure 1. Velocity plots are as described in Figure 3.

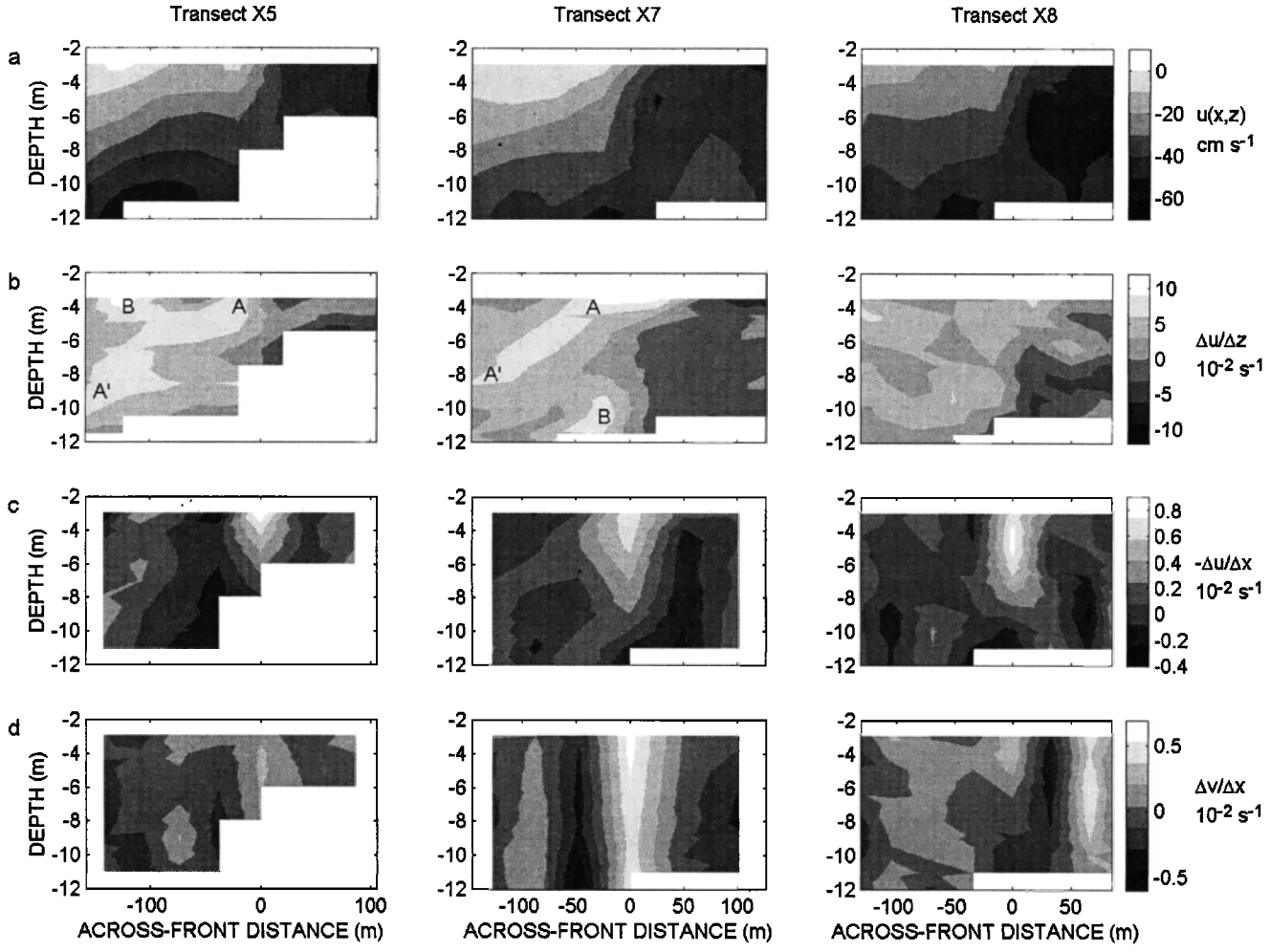

Figure 6. (a) Across-front velocity fields $u(x,z)$. (b) Velocity gradient fields for the vertical shear of across-front velocity. (c) Velocity gradient fields for the across-front convergence of across-front velocity. (d) Velocity gradient fields for the across-front shear of along-front velocity. All gradients are finite-difference estimates based on consecutive ADCP ensembles. The origin on the across-front distance axis is based on the location of strong across-front convergence in the frontal zone.

4.1. Vertical Shear and Dynamic Stability

Finite difference vertical shear estimates $\Delta u/\Delta z$, computed from the across-front velocity fields, are shown in Figure 6b. In general, the vertical shear in the flood current approaching the front from the seaward side ($x > 0$) was very weak compared with that on the upriver side of the front ($x < 0$). In transects X5 and X7, during which the front was visually well defined at the surface, strong shear was concentrated in relatively coherent layers marked AA' in Figure 6, sloping down from the surface at $x = 0$ and separating the nearly slack buoyant surface layer from the inflow proceeding as an intruding undercurrent below. Strong shear regions marked B branched off the main layer, near the surface in X5 and near the bottom in X7. In X8, when the foam line had disintegrated, strong vertical shear appeared in more isolated patches.

Underway during the cross-front transects, only ADCP velocity data were acquired, but at stations, CTD and ADCP profiles were sampled simultaneously. At stations on the upriver, stratified side of the front, S5 in Figure 3, S6 in Figure 5, and S8 (not shown), density varied approximately linearly across the shear layers. Turbulent transport across these stratified shear layers, a potentially significant element of cross-frontal exchange, will depend on the dynamic stability of the flow, which may be investigated in terms of the gradient Richardson number, $Ri = N^2/S^2$, where N is the buoyancy frequency, given by $N^2 = (-g/\rho)(\partial\rho/\partial z)$, g is acceleration due to gravity, ρ is density, and S is vertical shear, given by $S^2 = (\partial u/\partial z)^2 + (\partial v/\partial z)^2$. For each of the three upriver stations, velocity gradients over the shear layer were determined by least squares for each of five consecutive ADCP ensembles (100 s). Means of the five estimates were used to compute S, which was combined with N determined from the CTD cast to form Ri. Velocity magnitude averaged over the shear layer was also computed for each station.

Results are presented in Table 1, showing that while the speed of the current more than doubled during this accelerating portion of flood flow, vertical shear increased by only 14%. Stratification increased as well (nearly constant density difference across a decreasing vertical interval), so that variation of Ri was small. Consideration of an

Table 1. Shear Layer Parameters

Station	Time, LT	Mean Speed, cm s^{-1}	Shear, s^{-1}	Buoyancy Frequency, s^{-1}	*Ri*
S5	1536	26	0.070	0.031	0.20
S6	1630	49	0.076	0.039	0.26
S8	1715	62	0.080	0.048	0.36

appropriate *Ri* threshold for shear instability is taken up in section 5.1. Station S5, at which the lowest stability was indicated, was sampled between the times of transects X7 and X8.

4.2. Across-Front Convergence

Subsurface convergence fields in sections across the frontal zone are shown in Figure 6c, based on estimates $-\Delta u/\Delta x$ computed from ADCP transect data. In each section a prominent zone of locally intensified convergence magnitude was observed at the front near the top of the ADCP profiling range, decreasing sharply over horizontal scales of tens of meters, i.e., at scales approaching the horizontal resolution of the data.

Convergence at and just below the surface could not be measured by the ADCP, but the accumulation of buoyant matter such as foam, grass, and debris into a sharply defined line along the surface was consistent with convergent flow there. In other observations of fronts, including this one on other occasions, visible attributes not indicative of surface convergence such as a color change across the front are prominent as well. Here we are referring specifically to the line of collected material as the visible surface frontal line. In general, the paths of the transects of this study were chosen on the basis of these surface lines, and in every transect that crossed one, strong subsurface convergence (Figure 6c) coincided with visible indicators of surface convergence. However, in transect X8 the material marking the surface line had rapidly dispersed to such an extent that there was no longer a distinct visual boundary. With no surface guidance this transect was begun in the vicinity of the previous crossing and continued until we (somewhat unexpectedly) encountered the subsurface convergence zone shown in Figure 6c, apparently as strong and horizontally localized as before but with maximum convergence located slightly deeper. Transect X9 was similar to X8, but on X10 a clear visible boundary line of foam, etc., had redeveloped.

Correlated with the disappearance and subsequent reappearance of the visible frontal line of material at the surface were changes in the character of boat velocity records (Figure 7), determined for each transect from ADCP bottom-track data. Within each transect, constant engine speed was maintained, but significant changes in velocity over the ground were observed, presumably due to the influence of surface currents. For example, approaching the front ($t < 0$) on downriver crossing X6, the vessel proceeded against a weak opposing current and then slowed relatively abruptly after encountering the much stronger flooding current on the seaward side of the front ($t > 0$). Similarly, on upriver crossings X5 and X7 the vessel began the transects traveling with the strong current and then slowed at the front. Finite

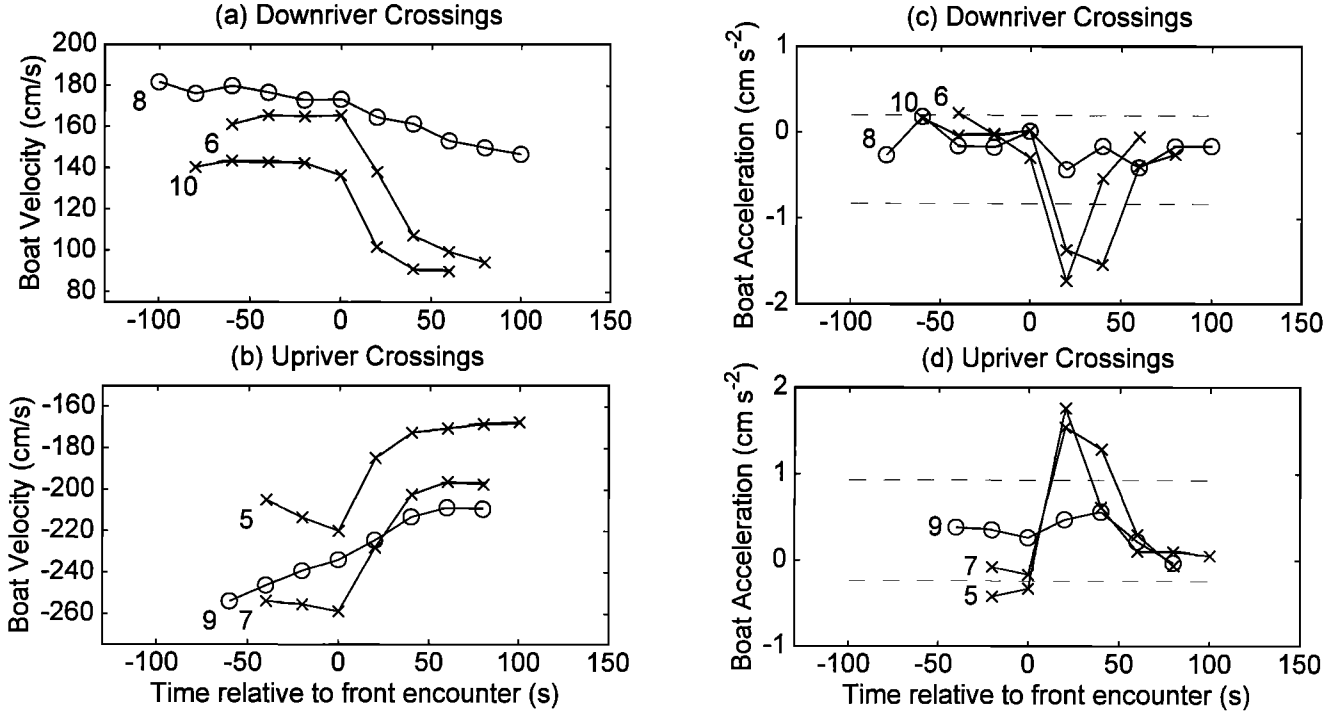

Figure 7. Time series of the across-front component of boat motion, determined by ADCP bottom tracking, on transects traveling downriver and upriver across the front: (a, b) boat velocity and (c, d) boat acceleration. The time origin corresponds to the encounter of strong across-front convergence several meters below the surface on each transect. Data denoted by crosses are from transects that crossed sharp lines of collected matter at the front. Data denoted by circles are from transects on which the surface material had been dispersed. In the boat acceleration time series the dashed lines indicate one standard deviation above and below the mean acceleration value.

difference boat accelerations between consecutive ensembles are also shown in Figure 7. The relatively strong accelerations occurred whenever, but only when, a visible frontal line well defined by collected matter was crossed. On transects X8 and X9, with no such line but during which across-front convergence was found well below the surface (Figure 6c), prominent acceleration of the boat did not occur. When continued tracking of the front became possible with the return of the surface line at the time of transect X10, a strong acceleration peak during the transect was again observed as well.

Existence of a sharp foam and debris line and the occurrence of abrupt vessel acceleration may both be associated with across-front convergence at the surface. The coherent presence, disappearance, and reappearance of both observed during this study would be consistent with a temporary disturbance of convergent flow at the surface, while subsurface convergence persisted, at least for a while.

4.3. Across-Front Shear of Along-Front Velocity

As with the convergence-type gradients just considered, the strongest variations of the along-front velocity component (v) in the across-front direction were generally concentrated in the frontal zone, as shown by the fields of horizontal shear estimates, $\Delta v/\Delta x$, in Figure 6d. From transect X5 to X7 the magnitude of shear across the front had increased by a factor of 2, with the strongest shear at the top of the ADCP profiles. As noted in section 3.2, the sharp foam line broke up shortly after X7, the remnants occupying a zone spanning most of the horizontal extent of the X8 fields. Possible association of the intensified horizontal shear with this disturbance is discussed in section 5.2. In transect X8, unlike X5 and X7, there was a region of strong horizontal shear that did not coincide with the strong convergence. Across-front horizontal shear was also measured by *Marmorino and Trump* [1996] with high resolution of the shear right at the front, whereas the present study documents the spatial distribution of the shear within the overall frontal zone.

5. Discussion

5.1. Stability of the Stratified Shear Flow

Shear instability (here referring to vertical shear, $\partial u/\partial z$) in the stratified layer upriver of the front is a potential mechanism for exchange of, for example, heat, salt, nutrients, or pollutants between the buoyant surface layer and the intruding inflow beneath it. Further, in a laboratory study of the frontal zone of a gravity current, *Britter and Simpson* [1978] concluded that such mixing across the shear layer between the two fluids is also an important process in determining the dynamics of a gravity current head. Corresponding to the mixing observed in a range of experiments, they measured a nearly constant layer Richardson number, $Ri_L = g'\Delta z/(\Delta U)^2$, where $g' = g\Delta\rho/\rho$ and ΔU, $\Delta\rho$, and Δz are the velocity, density, and depth changes across the shear layer. Constraining their analytical model with the condition $Ri_L = 0.35$, based on experiments by *Thorpe* [1973], led to good agreement between model solutions and their measured flow.

Geyer and Smith [1987] confirmed that the association between shear instability and critical Ri applies at natural estuarine scales by identifying the existence and structure of mixing in acoustic backscatter images, acquired simultaneously with velocity and density gradients. Their results suggested that the Richardson number at the threshold of instability was approximately 0.33, consistent with laboratory results, if based on mean shear (averaged over timescales that were long compared to the buoyancy period), and approximately 0.25, if based on instantaneous shear (including the contribution from internal waves).

To interpret our Ri estimates (Table 1) in the context of *Geyer and Smith's* [1987] results, the 0.25 threshold is probably more appropriate because our shear measurement interval (100 s) was shorter than the buoyancy period $2\pi/N$ (that is, the minimum internal wave period). Thus our results suggest that shear instability was likely when the front was near stations S5 and S6 but that the shear flow was marginally stable when sampled at station S8. Clearly, many more determinations of Ri, along with a means of detecting the signatures of shear instability, would be required to elucidate the role of this mechanism in tidal intrusion fronts. However, one of the effects of shear instability, according to Geyer and Smith, is that it tends to produce linear profiles of velocity and density, consistent with the measurements reported here (Figures 3 and 5).

5.2. Perturbation at the Surface

The execution of this field study was dependent to a large extent upon locating the moving front visually. Temporary loss of the visual identity took place when the line of collected material marking a sharply defined frontal boundary disintegrated and the existence of a recognizable "front" was no longer apparent on the surface, yet well-defined across-front convergence was measured 4–5 m below the surface. The study was interrupted for approximately 30 min until a clear foam line had formed again, providing the sampling guidance to continue the transects.

In this study, we have no information on what had accumulated and then dispersed at the front other than the conspicuous foam, grass, and debris. However, the very near surface waters at estuarine fronts are of particular interest because of the potential for flow convergence to bring about enhanced concentrations of buoyant plankton and pollutants, organic films, and surface-seeking larvae [*Mann and Lazier*, 1996, p. 207; *O'Donnell*, 1993; *Simpson and James*, 1986]. *Eggleston et al.* [1998] have recently investigated the role of estuarine fronts as possible barriers and eventual conduits for transport of crab larvae, which are found in surface waters. For a tidal intrusion front a natural overall timescale for its influence is the duration of the flood phase of the tide. However, in the present study the observed sequence of accumulation, dispersal, and renewed accumulation imposes shorter timescales on the system within the tidal cycle. Also, such temporary disruptions to organized surface concentrations that occur within the flood phase when the current is relatively strong may be rather different from and more energetic than the cessation of convergence associated with the ultimate senescence of a tidal intrusion front as the flood current becomes slack and reverses, or that of a plume front, as observed by *Garvine and Monk* [1974], when the supply of buoyant fluid is exhausted.

To assess the significance of the observed disturbance, further information on the frequency of occurrence of similar events would be required along with detailed velocity and

scalar data measured as near to the surface as possible while a cycle of disruption and reestablishment of surface accumulation is in progress. Instrument configurations used by *Marmorino and Trump* [1996] in a study of this intrusion front and by *O'Donnell* [1997] in a study of the Connecticut River plume front have appropriate capabilities and could be deployed with the objective of staying with a given branch of the front, with contingencies for sampling projected locations if the visible manifestation of the moving front is lost. Note that surface convergence is the basis for detection of fronts by radar remote sensing [*Marmorino and Trump*, 1996], so a major disruption could cause a loss of the expected surface signal for quantitative detection as well as for subjective visual identification.

Clearly, further field study would be required as well to establish the underlying cause of the observed disturbance at the surface. It may have been associated with an instability of the shear of the along-front velocity across the front $\partial v/\partial x$, which had intensified near the surface just prior to the event. Analysis of an idealized shear zone of horizontal width Δx shows that such a flow is unstable to horizontal oscillations with wavelength greater than $5\Delta x$ [*Cushman-Roisin*, 1994, p. 105] and that the fastest growing perturbations have wavelength $8\Delta x$ [*Drazin and Reid*, 1981, p. 146]. As noted by *Marmorino and Trump* [1996], the existence of simultaneous across-front convergence is not included in that analysis, and we may point out that neither is stratification or the vertical variation of $\partial v/\partial x$ that we observed. However, the basic result that the horizontally sheared flow is unstable to horizontal oscillations with wavelength "long" compared to the width of the shear zone may still apply. In fact, a sinuous appearance to the surface line of the James River front is fairly common and was described explicitly by Marmorino and Trump, but systematic documentation of that attribute was not carried out in the present study. An alternative to shear instability as the cause of the observed disturbance is that the front was adjusting to some flow changes associated with variations in bottom topography as it advanced up the estuary.

5.3. Downwelling in the Frontal Zone

By continuity, the convergence observed in the across-front velocity component at the front must be balanced by divergence in one or both of the other components. This and previous studies of the James River front suggest that in the along-front direction the velocity scale is smaller than that in the across-front direction and the length scale is larger than that in the across-front direction, and dye studies [*Kuo et al.*, 1988] have documented relatively strong downward flow at the front. Thus we assume that $\partial u/\partial x + \partial w/\partial z = 0$ is an adequate approximation of the continuity equation, and we use velocity profiles bracketing the front to make some estimates of $w(z)$, profiles of downwelling or subduction flow, in the frontal zone. Convergence estimates $\Delta u/\Delta x$ were integrated over the depth range spanned by the usable bins to find a profile of vertical velocity. In order to fix the profile with respect to a known value, namely, the boundary condition $w(z=0) = 0$, it was necessary to estimate the convergence above the shallowest ADCP bin, and vessel velocity records (Figure 7) were used for this purpose.

Resulting profiles of vertical velocity in the frontal zone, based on transects X5, when the front was over the steep bottom slope, and X11, when the front was upestuary over a more gradual slope, are shown in Figure 8. In both cases, the downward velocity magnitude increased rapidly with depth to middepth values of 3–5 cm s^{-1}. A schematic continuation of the profiles to the bottom is indicated by the lower dashed segments connecting the deepest continuity-based values to a bottom boundary value w_b based on no normal flow, i.e., $w_b = -u_b \partial h/\partial x$, where h is bottom depth and u_b is the horizontal velocity at the bottom, estimated here by averaging the deepest u values of the bracketing ADCP ensembles. Thus these near-bottom estimates of w are very crude and should be regarded as a rough approximation only, serving primarily to illustrate the relative influence of varying bottom slope. Note that if the interensemble spacing exceeds the actual horizontal length scale of the cross-front velocity transition, as it apparently does in some transects, then the measured values of $|\Delta u/\Delta x|$ underestimate $|\partial u/\partial x|$ and the magnitudes of vertical velocity determined here represent lower bounds.

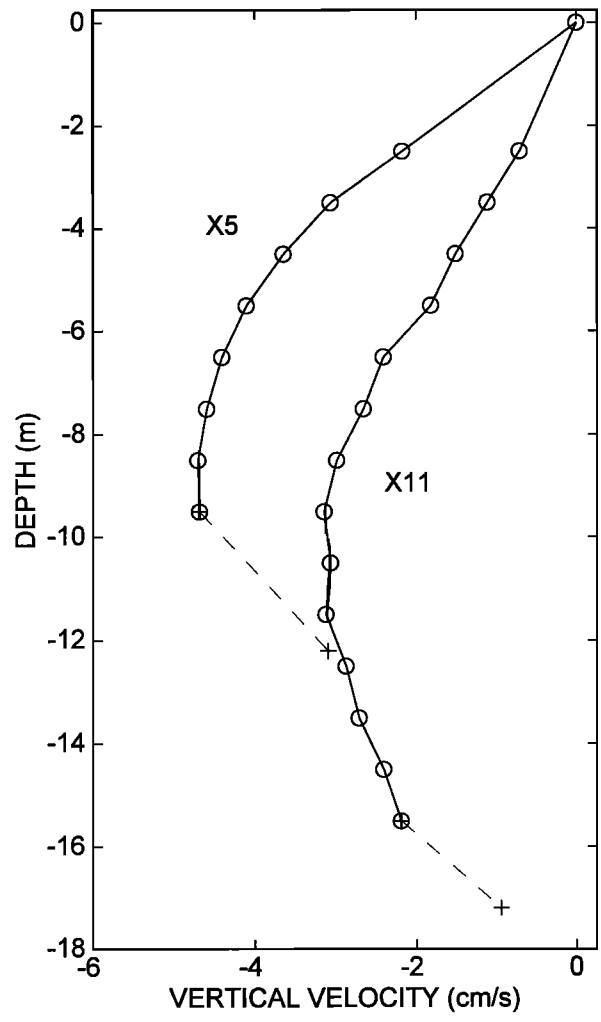

Figure 8. Profiles of vertical velocity in the frontal zone, derived from the continuity equation and the data from ADCP ensembles bracketing the front on transects X5 and X11. Because the interensemble spacing appeared to be greater than the actual length scale of horizontal convergence, the velocity magnitudes in these profiles represent lower bound estimates. Dashed segments are based on a boundary condition of no normal flow over the sloping bottom.

This is consistent with results of a subsequent, complementary study of this frontal system by *Marmorino and Trump* [1996], in which they measured vertical velocities of 15 cm/s.

6. Summary and Concluding Remarks

We have measured the velocity field in a plane locally perpendicular to a tidal intrusion front as it progressed upriver on the flooding tide. The characteristic structure of the observed flow field near the front was consistent with that portrayed schematically in Figure 2, including the location of subsurface features relative to the visible signs of the front on the surface.

The stratified shear layer (vertical variation of the across-front velocity) on the upriver side of the front was found to be at or near the threshold of shear instability, with cross-isopycnal mixing between the buoyant upper layer and the intruding underflow likely at times during our observations. More thorough investigation of this shear flow would be useful, with attention to the variation of stability with distance upriver from the front and an assessment of intermittency in the occurrence of instability.

We observed a buildup in horizontal shear across the front (across-front variation of the along-front velocity), with intensity increasing toward the surface. Possibly, but not necessarily, connected to this shear was the subsequent dispersal of the sharply defined narrow line of collected material on the surface into widely scattered fragments. The disruption to the characteristic accumulating action at the surface was temporary and appeared to be of vertically limited extent, rendering the frontal location invisible at the surface while highly localized convergence continued at depths of several meters for at least 10 min following the surface breakup (sampling was then interrupted). To explore the dynamics of such events and the relevance of intratidal cycles of concentration and scattering in near-surface waters in estuarine environments where tidal intrusion fronts form, sampling strategies specifically anticipating loss of surface detectability of the moving frontal zone will be required.

Relatively strong across-front convergence, concentrated in the frontal zone, was a characteristic feature of the measured velocity fields. By continuity considerations the vertical structure of the convergence implied a downward flow in the frontal zone, accommodated at depth by a combination of divergent flow in the across-front direction and a bottom boundary sloping downward in the direction of flow. Because the sampling did not fully resolve the sharpness of the frontal transition, the magnitudes of the convergence and vertical velocity estimates are reported here as lower bounds.

Instabilities, both of the stratified shear flow upriver of the front and of undetermined origin along the front at the surface, may play a role in cross-front exchange. Further work to verify and quantify fluxes associated with these mechanisms would be of particular interest because in an estuarine flow, cross-frontal exchange may also imply exchange between net seaward flow of surface waters and net upestuary flow at deeper levels. Indeed, part of the motivation for investigating this frontal system stemmed from interest in its role in the retention of bivalve larvae in the James River [*Mann*, 1988; *Kuo et al.*, 1990b].

Appendix

Resolution capabilities of the ADCP in vertical distance, horizontal velocity, and time are interdependent. According to the manufacturer, *RD Instruments* [1991], an estimate of a horizontal velocity component based on an ensemble average of n pings has a standard deviation given by

$$\Delta u = \frac{a}{f\Delta z\sqrt{n}}$$

where f is the transmitted frequency (hertz), Δz is the vertical (not along-beam) cell length (meters), and for a standard four-beam narrowband ADCP with beams inclined 30° from vertical, $a = 1.6 \times 10^5$ m^2 s^{-2}. If over an ensemble time interval Δt the average ping rate is given by r (pings per second), then $n = r\Delta t$ and the resolution tradeoffs can be summarized in a triple "uncertainty principle"

$$\Delta u\Delta z\sqrt{\Delta t} = \frac{a}{f\sqrt{r}}$$

For underway measurement at vessel speed U the horizontal sampling interval is $\Delta x = U\Delta t$, and the uncertainty relation is

$$\Delta u\Delta z\sqrt{\Delta x} = (a/f)\sqrt{U/r}$$

Some constraints are implicit in this expression. Long-term bias in ADCP velocity measurements is approximately 0.005–0.01 m s^{-1}, so there is no benefit in reducing the short-term error Δu below this level. The minimum available depth cell length Δz for the 1.2-MHz narrowband ADCP is 1 m. The value Δx cannot be regarded as a meaningful measure of horizontal resolution at depths where the horizontal separation of opposing ADCP beams (L) is comparable to or greater than Δx (with beam angle θ, $L = 2D \tan\theta$ at vertical range D). Requirements of synopticity and vessel maneuverability may impose a minimum U, while maximum ping rate r will depend on water depth, data transmission rate, and data acquisition software. Subject to all these limitations, once the right-hand side has been minimized for particular operating conditions, the quantities on the left-hand side can be adjusted in various resolution tradeoffs. Significant improvements in the overall resolution product have been achieved in the broadband ADCP. The limitation on Δx due to beam separation still applies but to a lesser extent because the typical beam angle for the broadband is 20° off vertical compared with 30° for the narrowband ADCP.

In this exploratory study we used $\Delta t = 20$ s, $r \approx 2$ pings per second, $\Delta z = 1$ m, giving $\Delta u \approx 0.021$ m s^{-1} for measured profile velocities in each recorded ensemble. Use of bottom tracking to determine absolute velocities introduces a small additional uncertainty; from the instrument specifications we estimate a combined statistical uncertainty, including bottom tracking, of 0.022 m s^{-1}. At CTD stations, with $\Delta t = 60$ s, the combined statistical uncertainty is 0.012 m s^{-1}. Horizontal resolution underway at vessel speeds of 1–2.5 m s^{-1} was $\Delta x =$ 20–50 m for the ensemble time interval of 20 s. Because the frontal transition appeared as a near discontinuity between consecutive ADCP ensembles (e.g., 100–101 on transect X5 in Figure 4), smaller Δx is desirable and could be achieved, we feel, through reduction in U/r without increasing Δu or Δz and also through the smaller single-ping uncertainty of the broadband ADCP.

Acknowledgments. We thank C. Machen for skillful and cooperative handling of the R/V *Langley*, J. Fryling and J. McNabb (representing RD Instruments) for providing the ADCP and overseeing its operation, and J. Posenau and W. Matthews for deploying and operating the CTD and Del Norte positioning instrumentation. Funding for this project was provided by the Virginia Institute of Marine Science. We are grateful for several helpful comments from an anonymous reviewer. This paper is contribution 2209 of the Virginia Institute of Marine Science, The College of William and Mary.

References

Bowman, M. J., Estuarine fronts, in *Hydrodynamics of Estuaries*, edited by B. J. Kjerfve, pp. 85-132, CRC Press, Boca Raton, Fla., 1988.

Britter, R. E., and J. E. Simpson, Experiments on the dynamics of a gravity current head, *J. Fluid Mech., 88*, 223-240, 1978.

Byrne, R. J., A. Y. Kuo, R. L. Mann, J. M. Brubaker, E. P. Ruzecki, P. V. Hyer, R. J. Diaz, and J. H. Posenau, New Port Island: An evaluation of potential impacts on marine resources of the lower James River and Hampton Roads, *Spec. Rep. Appl. Mar. Sci. Ocean Eng. 283*, 276 pp., Va. Inst. of Mar. Sci., Gloucester Point, 1987.

Cushman-Roisin, B., *Introduction to Geophysical Fluid Dynamics*, 320 pp., Prentice-Hall, Englewood Cliffs, N. J., 1994.

Drazin, P. G., and W. H. Reid, *Hydrodynamic Stability*, 525 pp., Cambridge Univ. Press, New York, 1981.

Eggleston, D. B., D. A. Armstrong, W. E. Elis, and W. S. Patton, Estuarine fronts as conduits for larval transport: Hydrodynamics and spatial distribution of Dungeness crab postlarvae, *Mar. Ecol. Prog. Ser., 164*, 73-82, 1998.

Garvine, R. W., An integral hydrodynamic model of upper ocean frontal dynamics, 1, Development and analysis, *J. Phys. Oceanogr., 9*, 1-18, 1979.

Garvine, R. W., and J. D. Monk, Frontal structure of a river plume, *J. Geophys. Res., 79*, 2251-2259, 1974.

Geyer, W. R., and J. D. Smith, Shear instability in a highly stratified estuary, *J. Phys. Oceanogr., 17*, 1668-1679, 1987.

Joyce, T. M., On in situ "calibration" of shipboard ADCPs, *J. Atmos. Oceanic Technol., 6*, 169-172, 1989.

Kuo, A. Y., R. J. Byrne, J. M. Brubaker, and J. H. Posenau, Vertical transport across an estuary front, in *Physical Processes in Estuaries*, edited by J. Dronkers and W. van Leussen, pp. 93-109, Springer-Verlag, New York, 1988.

Kuo, A. Y., R. J. Byrne, P. V. Hyer, E. P. Ruzecki, and J. M. Brubaker, Practical application of theory for tidal intrusion fronts, *J. Waterw. Port Coastal Ocean Eng., 116*, 341-361, 1990a.

Kuo, A. Y., E. P. Ruzecki, B. J. Neilson, J. M. Brubaker, and R. J. Byrne, Circulation and transport of oyster larvae in Virginia estuaries, in *Physics of Shallow Seas*, edited by W. Huatong, W. Jingyong, and D. Hua, pp. 41-51, China Ocean Press, Beijing, 1990b.

Largier, J. L., Tidal intrusion fronts, *Estuaries, 15*, 26-39, 1992.

Largier, J. L., Estuarine fronts: How important are they?, *Estuaries, 16*, 1-11, 1993.

Largier, J. L., and S. Taljaard, The dynamics of tidal intrusion, retention, and removal of sea water in a bar-built estuary, *Estuarine Coastal Shelf Sci., 33*, 325-338, 1991.

Mann, K. H., and J. R. N. Lazier, *Dynamics of Marine Ecosystems: Biological-Physical Interactions in the Ocean*, 2nd ed., 394 pp., Blackwell Sci., Cambridge, Mass., 1996.

Mann, R., Distribution of bivalve larvae at a frontal system in the James River, Virginia, *Mar. Ecol. Prog. Ser., 50*, 29-44, 1988.

Marmorino, G. O., and C. L. Trump, High-resolution measurements made across a tidal intrusion front, *J. Geophys. Res., 101*, 25,661-25,674, 1996.

McClimans, T. A., Estuarine fronts and river plumes, in *Physical Processes in Estuaries*, edited by J. Dronkers and W. van Leussen, pp. 55-69, Springer-Verlag, New York, 1988.

O'Donnell, J., Surface fronts in estuaries: A review, *Estuaries, 16*, 12-39, 1993.

O'Donnell, J., Observations of near-surface currents and hydrography in the Connecticut River plume with the surface current and density array, *J. Geophys. Res., 102*, 25,021-25,033, 1997.

RD Instruments, Direct-reading acoustic Doppler current profiler (DR-ADCP) technical manual, San Diego, Calif., 1991.

Ruzecki, E. P., and W. J. Hargis, Interaction between circulation of the estuary of the James River and transport of oyster larvae, in *Estuarine Circulation*, edited by B. J. Neilson, A. Kuo, and J. Brubaker, pp. 255-278, Humana Press, Totowa, N. J., 1989.

Simpson, J. H., and I. D. James, Coastal and estuarine fronts, in *Baroclinic Processes on Continental Shelves, Coastal Estuarine Sci*, vol. 3, edited by C. N. K. Mooers, pp. 63-93, AGU, Washington, D.C., 1986.

Simpson, J. H., and R. A. Nunes, The tidal intrusion front: An estuarine convergence zone, *Estuarine Coastal Shelf Sci., 13*, 257-266, 1981.

Thorpe, S. A., Experiments on instability and turbulence in a stratified shear flow, *J. Fluid Mech., 61*, 731-751, 1973.

J. M. Brubaker, School of Marine Science, Virginia Institute of Marine Science, College of William and Mary, P.O. Box 1346, Gloucester Point, VA 23062-1346. (brubaker@vims.edu)

J. H. Simpson, School of Ocean Sciences, Marine Science Laboratories, Menai Bridge, University of Wales, Anglesey LL59 5EY, Wales, U.K.

(Received February 13, 1997; revised August 11, 1998; accepted October 15, 1998.)